Fe- and Co-based HVAF-sprayed coatings: Characterization and electrochemical properties

E. Sadeghimeresht[a]*, **N. Markocsan[a]**, **P. Nylén[a]**, **S. Dizdar[b]**

[a] Production Technology Centre, University West, 461 53 Trollhättan, Sweden

[b] Höganäs AB, 263 83 Höganäs, Höganäs, Sweden

Abstract

Two types of Fe-based and one type of Co-based coatings with chemical compositions (in wt.%) Fe-28Cr-16Ni-1.85C (FeNiCrC), Fe-17Cr-12Ni (FeNiCr) and Co-28Cr-1C (CoCrC) were sprayed by HVAF technique. The effect of alloying element, coating thickness, and in-flight particle temperature on corrosion behavior of the coatings were comparatively studied by SEM/EDS, XRD, and electrochemical testing. OCP, polarization and EIS tests were performed in 3.5 wt.% NaCl solution at 25°C. Polarization tests showed that FeCrNiC coating protected the underlying substrate better than CoCrC coating, while FeCrNi coating failed to hinder the penetration of corrosive ions. EIS measurements revealed that the solution penetrated into the coating through the defects, however the corrosion process slowed down due to the clogging of the interconnected defects by corrosion products. Increasing the in-flight particle temperature from 1400°C to 1515°C led to a denser coating with less defect which eventually improved the corrosion resistance of FeCrNiC coating.

* Corresponding author, E-mail: Esmaeil.sadeghimeresht@hv.se.

1. Introduction

Corrosion is a serious problem in many industrial components, resulting in catastrophic failure, economic loss, and personal injury [1-3]. To address these problems, many efforts have been performed to produce high-performance Co-based coatings with improved corrosion behavior [4]. However, the drawbacks of Co in terms of cost and environmental restriction have made it necessary to produce more adapted protective coatings [5-9]. High-alloyed Fe-based coatings containing sufficient level of major alloying element e.g., Cr and Ni could be a cheap and environmentally friendly alternative to the state-of-the-art Co-based coatings in such a condition that coatings with high functionality are demanded [5, 10-13]. Moreover, high-alloyed Fe-based alloys with adding minor alloying elements e.g., C or B are also designed to enhance both corrosion and wear resistance capabilities of the coatings [14-22].

Thermal spraying, which is extensively used to protect the substrate in harsh corrosive environments, is capable of meeting the demands in production of high quality coatings. Among several thermal spraying techniques, high-velocity air/fuel (HVAF) is a well-developed thermal spray process that has recently received increased attention as a better alternative to electrolytic hard chromium (EHC) compared with high-velocity oxy/fuel (HVOF) [11, 23-25]. Interestingly, HVAF technique brings notable advantages in terms of cost and coating properties [24, 26-28]. The high velocity of the in-flight particles (1000-1200 m/s) enables a generation of dense coatings with low porosity [29]. Moreover, low spraying temperature (below 1950°C) and short particle dwell time lead to minimal feedstock phase transformation and almost inexistent elemental depletion/decomposition of in-flight particles. Furthermore, replacing pure oxygen in HVOF process with air in HVAF, significantly reduces the formation of oxides within the coatings, while still retains its ability to produce high performance coatings [27, 30]. Among a few attempts made to fabricate Fe-based coatings by HVAF process [2, 19, 24, 28, 36, 37], most of the coatings have presented excellent properties, particularly superior corrosion behavior in

different environments such as acid, alkaline, and chloride solutions. High quality microstructure including low oxide content, high retention of powder microstructure and dense of HVAF-sprayed Fe-based coatings were reported in [10].

Several studies have been concentrated on Co-based coatings (mostly driven by the automotive industry), however less attention paid to the low temperature corrosion behavior of thermally sprayed Fe-based coatings. While many corrosion studies are concerned using amorphous Fe-based powder [28, 33], the others are focused on Fe-based alloys with complex chemical composition by adding beneficial elements such as Cr [32]. Cr is initially added to provide sufficient Cr dissolved in the austenitic (γ) solid solution matrix to increase the ability of the alloy to form a thin protective surface oxide layer and secondly to form hard precipitates in the presence of C to provide a wear resistance coating. Therefore, high Cr content in the alloy favors the coating to have both corrosion and wear resistance [33].

Promising results were obtained with the HVAF process [36], but corrosion behavior of high- and low-alloyed Fe-based coatings produced by HVAF as a potential alternative to Co-based coatings have not yet been surveyed. In the present study, both Fe- and Co-based coatings were deposited by HVAF technique and their microstructure and corrosion behavior were comparatively investigated. Corrosion properties were studied with open-circuit potential (OCP), polarization and electrochemical impedance spectroscopy (EIS) measurements, and the role of corrosive species and the type of corrosion products were evaluated by SEM/EDS and XRD.

2. Experimental

2.1. Material and method

2.1.1. Substrate material

Domex 355 steel (0.10C- 0.03Si- 1.50Mn- 0.02P- 0.01S- 0.20V- 0.15Ti wt.%) in the shape of a ring was used as the substrate material. The ring with an inside diameter of 100 mm and a thickness of 2 mm were fixed on a rotating carousel and coated with sequential spray passes.

Before spraying, the substrates were degreased in acetone and, then, grit blasted with alumina grits (mesh 220) to clean and roughen the surface. Before each corrosion testing, the samples were cut to the size of 10×10×2 mm^3, degreased and rinsed in high-purity water, followed by ethanol- and air-drying.

2.1.2. Coating materials

Three gas-atomized Fe- and Co-based powders with the particle size between 20 and 53 μm were used in this study. The exact chemical composition as well as density of the powders are presented in Table 1.

Table 1. Powder composition and apparent density

Powder	Composition (wt.%)									Apparent density
	Cr	Ni	C	W	Si	Mo	Mn	Fe	Co	(g/cm^3)
1	28.0	16.0	1.85	-	1.2	4.4	1.5	Bal.	-	4.2
2	17.0	12.0	0.01	-	-	2.5	1.5	Bal.	-	4.1
3	28.0	1.5	1.00	4.4	1.1	-	-	0.5	Bal.	4.6

2.2. Solution preparation

The experiments were performed in 3.5 wt.% NaCl (seawater) solution. All the chemical solutions were used from analytical grade reagents with distilled water. While the solutions were in equilibrium state with the atmosphere, all the experiments were carried out under thermostatic conditions (25±0.1°C).

2.3. Thermal spraying experiments

For grit blasting the substrates, standard configuration of the HVAF-M3 system was used, i.e. long nozzle, large combustion chamber, short axial powder injector, utilizing DURALUM

White F220 alumina powder (mesh 220), and combustion gas of propane. A number of spray parameter sets were initially employed and tested to reach the final and optimized process parameters presented in Table 2. The coatings were sprayed while the substrate rotating and HVAF torch kept fixed. Thus, the thickness of the coatings was roughly controlled through the number of sample rotations. Six different sets of Fe- and Co- based coatings were produced on the steel substrate based on Table 3. These sets enabled us to identify the effect of Fe- and Co-based coating on corrosion behavior. Furthermore, the effect of different alloying elements, coating thicknesses, and in-flight particle temperature on corrosion behavior of the coatings could be also studied.

Table 3. HVAF process parameters used in this study

Parameter	Value
Spray distance (mm)	350
Gun traverse velocity (m/min)	100
Powder feed rate (g/min)	150
Nitrogen carrier gas flow (l/min)	60

Table 3. Various types of coatings produced in this study

Coding	Powder used	In-flight particle temperature (°C)	Thickness*
FeCrNiC1	Fe-based powder 1	1515	Low
FeCrNiC2	Fe-based powder 1	1515	High
FeCrNiC3	Fe-based powder 1	1400	High
FeCrNi	Fe-based powder 2	1400	High
CoCrC1	Co-based powder 3	1400	Low
CoCrC2	Co-based powder 3	1400	High

*The exact values of thickness were measured later using optical microscopy

2.4. Porosity, microhardness and surface roughness measurements

The image analysis technique was used to measure the porosity content in the coatings by converting the microstructure images of the coatings into binary images and quantifying the percentage of dark areas. The image analyzer software ImageJ [37], was utilized for the measurements. Surface roughness was measured using a surface roughness recorder (Surftest 301, Mitutoyo, Japan). Micro-Vickers hardness measurements were carried out on the polished cross section of the coatings according to ASTM E384-10 with a Vickers indenter at the load of 300 g and the dwell time of 15 s using a Shimadzu Microhardness Tester.

2.5. Corrosion tests

2.5.1. OCP, Potentiodynamic polarization and EIS measurements

The corrosion behavior of HVAF-sprayed coatings was studied with OCP, potentiodynamic polarization and EIS techniques. As-sprayed coatings without any further treatments e.g., polishing were used in order to keep the initial surface roughness and possible defects in the top layer of the coating. OCP measurements were carried out by gluing a plastic tube (φ=20mm) to the coating surface. 20 ml of a 3.5 wt.% NaCl solution was poured into the tube. The OCP was measured up to 24 hours of immersion.

Polarization and EIS evaluations were carried out in a conventional three-electrode cell with the counter electrode of platinum foil, the as-sprayed coating as the working electrode (WE) and the reference electrode of saturated calomel electrode (SCE). The surface area of the coatings exposed to the electrolyte was 0.2 cm^2. Before each electrochemical measurement, the samples were immersed in the electrolyte at the open-circuit potential for 1 h to be adequate to acquire a steady state. The polarization curves were generated by scanning the potential range that varied from -250 to +2000 mV (vs. OCP) at the scanning rate of 1.0 mV/s, using a computer-controlled potentiostat/galvanostat (IVIUMSTAT). The Zview program was used for calculations of anodic (β_a) and cathodic (β_c) Tafel constants required for polarization resistance

calculations. The polarization resistance (R_p) of coatings was calculated by using the Stern–Geary eq. (1) [38]:

$$R_p = \frac{d\mathrm{E}}{d\mathrm{i}} = \frac{1}{i_{corr}} \frac{\beta_a \beta_c}{2.303(\beta_a + \beta_c)} \tag{1}$$

where i_{corr} is the corrosion current density, β_a and β_c are the slope of anodic and cathodic Tafel lines respectively.

EIS studies were also performed using IVIUMSTAT with the AC amplitude of the sinusoidal deviation of ±10 mV and measurement frequency between 10 and 100 kHz around the OCP measured for 30 s before EIS measurement. The computer system was equipped with an IVI-UMSTAT software analyzer to record EIS data and the Zview program to determine the numerical values of the parameters of the suggested electric circuit model. Fresh sample and fresh solution were used for each exposure.

2.6. Coating characterization

Cross-sections of the coating systems were metalographically prepared for microstructure analysis. The morphology of the specimens was characterized using a QUANTA 200 FEG scanning electron microscope (SEM) and X-ray energy dispersive spectroscopy (EDS). The phases present in the top and bond coatings before and after the corrosion tests were identified by X-ray diffraction (XRD) utilizing Siemens D500 X-ray Diffractometer with Cu K$_\alpha$ radiation (λ=0.154 nm) operating with the diffraction angle (2θ) varied between 25° and 85°.

3. Results and discussion

3.1. Characterizing the coatings

The cross-sectional optical micrographs of the as-sprayed Fe- and Co-based coatings are presented in Fig. 1(a-f). Morphology of all coatings showed the characteristics of lamellar structures with the elongated axis of impacted splats firmly aligned with the substrate surface. The lamellar structure was more visible in FeNiCr coating showed that the low-alloyed Fe-based powder was melted better during spraying.
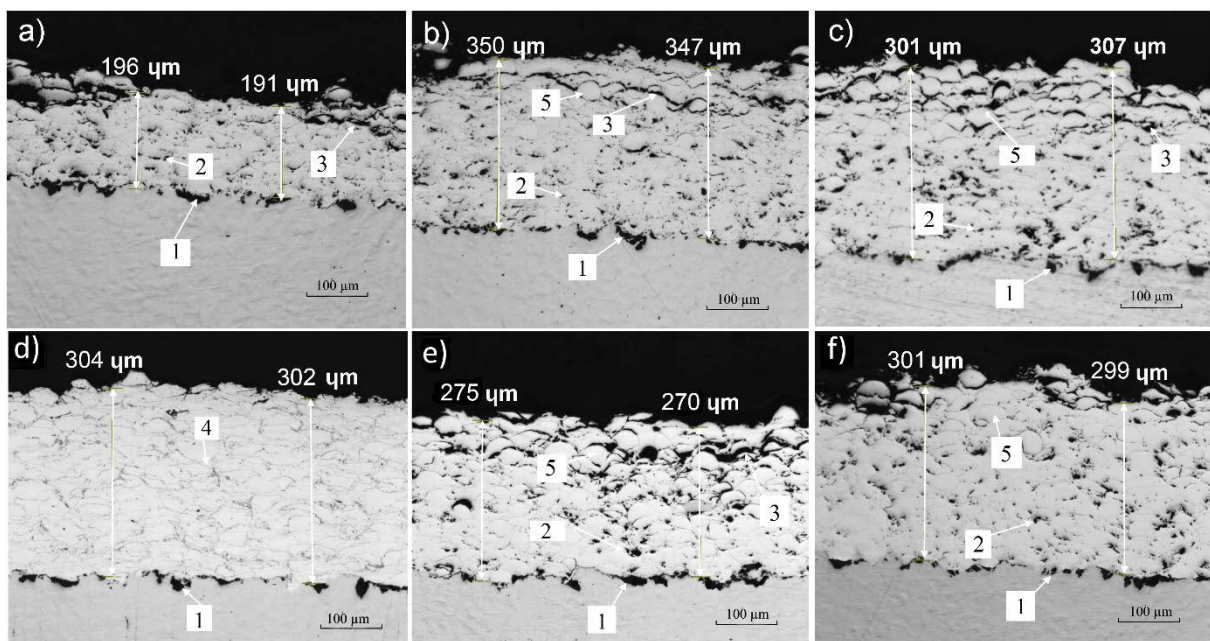

Fig. 1. OM micrographs of as-sprayed coatings, a) FeCrNiC1, b) FeCrNiC2, c) FeCrNiC3, d) FeCrNi, e) CoCrC1, and f) CoCrC2, (Features of the coatings: 1: Embedded grit blasting Al_2O_3 particles, 2: Pores, 3: Cracks, 4: Lamellar structure, 5: Unmelted or semimelted particles).

The porosity is an important parameter that can define the performance of thermal spray coatings, mainly in term of corrosion. The porosities permit the electrolyte to penetrate and attack the substrate chemically [40]. The porosity level was low for FeCrNi, reaching the maximum of 0.1%, while the value was measured around 2.6%, 2.2%, and 4.7% for FeCrNiC coatings 1, 2, and 3 respectively. In CoCrC1, porosity content was around 2.9%, whereas in CoCrC2, the value of 2.2% was obtained. It showed that the densest coating was produced from low-alloyed

Fe-based coating. Moreover, increasing the in-flight particle temperature from 1400°C in FeCrNiC3 (Fig. 1 c) to 1515°C in FeCrNiC2 (Figs. 1 a and b) led to a decline in the mean diameter of the deposited particles and resulted in the denser microstructure.

Fig. 2 showed the SEM cross-sectional images of the coatings. All coatings exhibited a porous structure on near-surface regions, however porosity was not critical for corrosion resistance, as pores were shallow and disconnected (at least at the bottom of the coating, where the coating was well-attached to the substrate) and the corrosive ions probably could not penetrate deep to reach the substrate/coating interface [7]. Furthermore, there are always a compromise among coating microstructure, feedstock characteristics, and coating properties. The defects e.g., porosity, or oxide might be compromised by the chemical composition of the coating in terms of coating properties, particularly corrosion, by adding some effective elements, e.g., Cr, Mo or Ni, which are able to present some possibilities to reduce corrosion.
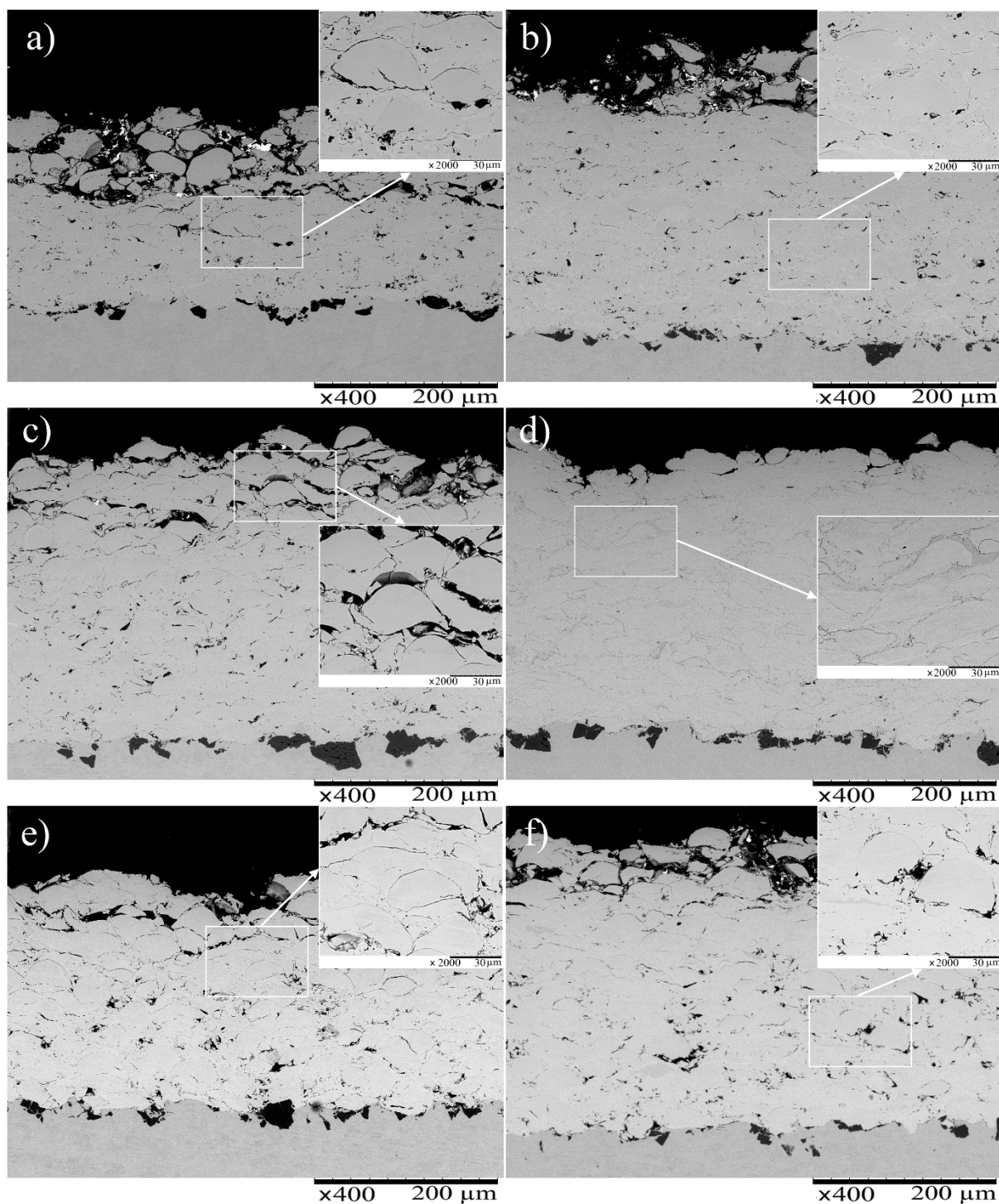
Fig. 2. Cross sectional SEM micrographs of as-sprayed coatings, a) FeCrNiC1, b) FeCrNiC2, c) FeCrNiC3, d) FeCrNi, e) CoCrC1, and f) CoCrC2.

Thickness, surface roughness and microhardness of the coatings are given in Table 4. The results in the table were the average of thirty measurements done on three different samples of each coating.

Table 4. Coating thicknesses, surface roughness, and microhardness

Coding	Thickness (µm)	Roughness (µm)	Microhardness ($HV_{0.3}$)
FeCrNiC1	183.3±10.6	6.1±0.6	631.7±20.1
FeCrNiC2	378.2±7.9	5.7±0.8	658.3±26.3
FeCrNiC3	303.9±3.2	8.9±0.3	610.7±14.7
FeCrNi	308.8±8.3	5.3±0.5	350.3±10.2
CoCrC1	272.2±12.9	8.1±0.6	863.1±18.9
CoCrC2	315.1±5.5	7.2±0.3	833.3±15.1

The surface roughness is important in term of corrosion protection, as the lower surface roughness leads to a lower surface area exposed to corrosive environment, which can result in less susceptibility to both general and localized corrosion [42]. Maximum value of roughness in FeCrNiC3 (8.9 µm) showed higher the susceptibility to uniform and localized corrosion compared to FeCrNi (5.3 µm), which had the smoother surface. It is worth noting that lower coating roughness in HVAF process can be achieved by increasing both particle velocity and flame temperature (before the critical point that phase transformation occurs) [24].

For the maximized protection of the substrate, thermal spray coatings has to be a dense and defect-free coating in order to prevent the corrosive ions to penetrate through defects (connected pores and cracks) and reach the substrate [43]. In this case, localized corrosion such as pitting and crevice may occur autocatalytically [44]. Fe-based coatings free of defects could not be probably achieved because of the inherent characteristics of the thermal spraying process. For instance, Cr content of the alloy might rapidly oxidize during spraying (due to a great susceptibility of Cr to oxidation). Formation of chromium oxides within the spraying consumes Cr which could be used later in corrosion prevention by formation of the surface passive layer. Therefore, Cr-depletion zones are formed due to the lack of sufficient available Cr which finally leads the coating to be corroded [45]. Thus, increasing the level of accessible Cr in the coating could improve the corrosion behavior. Altering the thickness of the coating is also reported as

a way that can reduce the rate of corrosive ion penetration through defects [24]. Thinner coating permits the electrolyte to meet the substrate through the coating defect, as it is not sufficiently thick to protect the substrate, unless the chemical composition of the coating (presence of alloying elements such as Cr) compromises the detrimental effect of the defects.

The microhardness of FeCrNiC coatings of 1, 2, and 3 were 631.7, 658.3, and 610.7 $HV_{0.3}$, respectively. The presence of carbon in the coatings that contains Cr increased the hardness due to the formation of carbides, particularly Cr_2C_3. The average microhardness in CoCrC1 and CoCrC2 were 863.1 and 833.3 $HV_{0.3}$, respectively. Higher hardness of these two coatings could be attributed to cobalt itself (Co is inherently harder than Fe), inclusions of cobalt oxides, fine microstructure of individual lamellae, and the presence of some types of carbides, mainly Cr_2C_3, due to presence of C and Cr in the feedstock Co-based powder. High scattering in microhardness values, which might be due to the presence of heterogeneities in the composition of coatings and inhomogeneity of the microstructure, enhances the coating sensitivity to some certain types of corrosion, particularly microgalvanic corrosion.

Phase identification of XRD patterns (Fig. 3) illustrated the presence of austenitic (γ) matrix in Fe-based coating, Co phase in Co-based coatings. The presence of slight martensitic phase was also detectable which might be due to the high cooling rate of the semimelted particles during the solidification. The σ-FeCr phase, which is susceptible to be formed in low cooling rate of the particles was not observed. Moreover, a small presence of Cr_2O_3 was assumed due to the increase of the low intensity peak at 38°. The XRD was unable to identify the presence of more oxides, much likely due to the high roughness of the coatings [4].
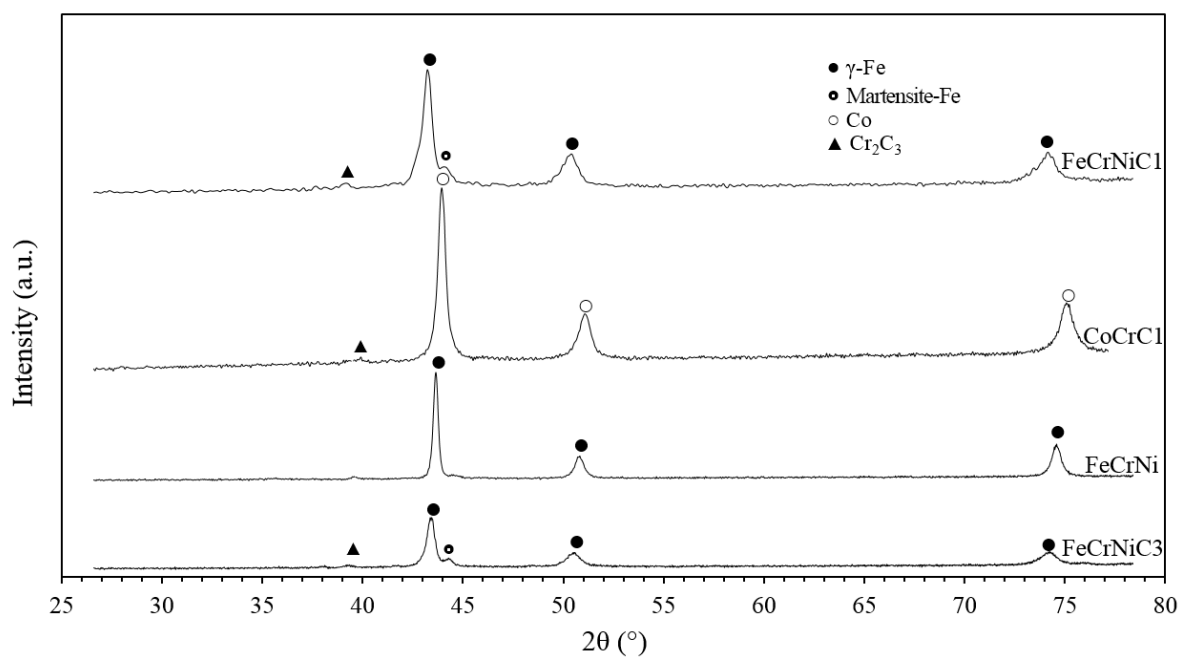
Fig. 3. XRD patterns of as-sprayed coatings.

3.2. OCP

The penetration of the corrosive species of the electrolyte along the coating thickness towards the substrate was evaluated by OCP measurements up to 24 hours of immersion (Fig. 4). The noble potential values were detected for the Fe-based coatings (FeCrNi and FeCrNiC1), while the negative values were recorded for Co-based coatings. This behavior showed that Fe-based coatings presented better barrier effect compared to Co-based coatings, which was probably attributed to the lack of interconnected porosities.
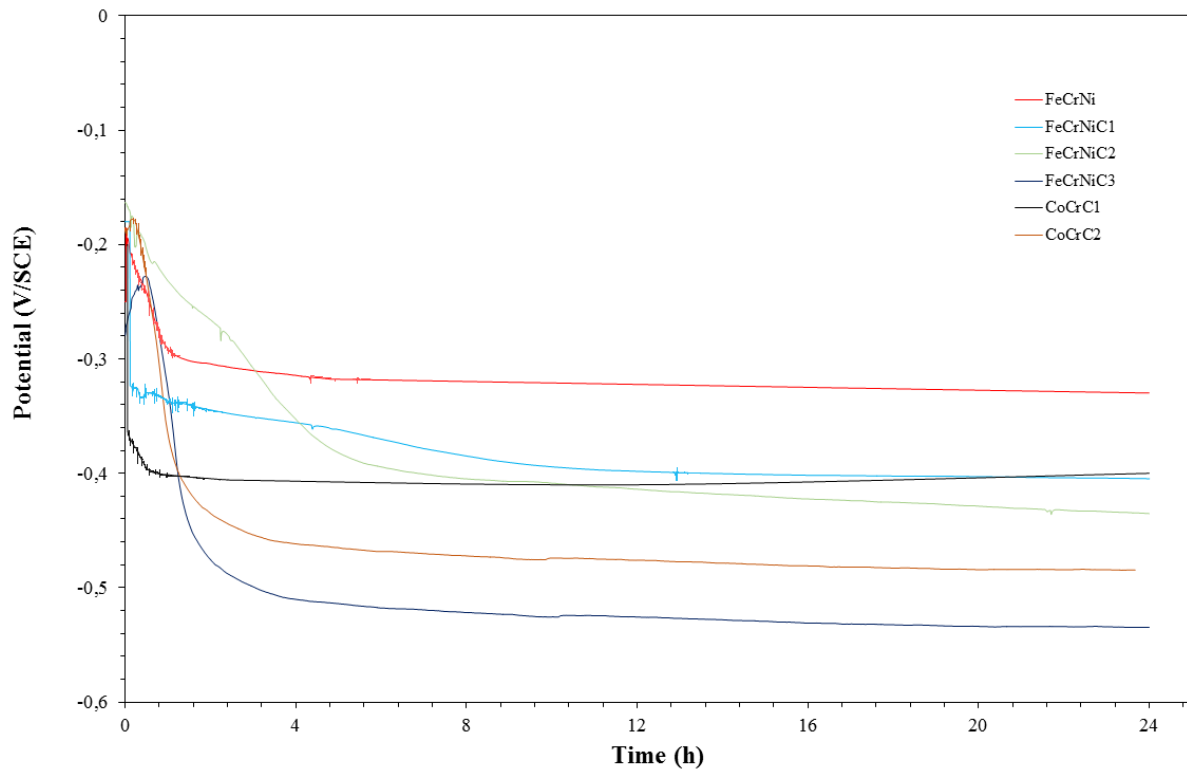
Fig. 4. OCP plots of various coatings over 24 h in 3.5 wt.% NaCl, at 25°C.

At the very early stage of the test, both Co-based coatings showed an initial low potential, which slowly increased and later followed by a decrease over time. This drop was also detected for the other coatings while the test started. The initial potential decrease can be associated with; 1) the variation in the surface activity primarily due to the electrolyte penetration along the coating, and 2) the dissolution of the initial oxide layer, which was naturally formed, after immersion into the electrolyte. The decrease of potential after the first hours, confirmed the penetration of the corrosive ions through open porosity or localized defect. However, after such a drop, the potential became steady probably due to clogging of open-pores rather than the passivation of the coating. Some frequent potential oscillations suggested the susceptibility of the coatings to localised corrosion such as pitting.

3.3. Potentiodynamic measurements

Fig. 5 showed the potentiodynamic polarization plots of various coatings immersed in 3.5 wt.% NaCl at 25°C, to know the overall kinetic of corrosion process. All the electrochemical parameters including the corrosion potential (E_{corr}), corrosion current density (i_{corr}), anodic (β_a) and cathodic (β_c) Tafel slopes and polarization resistance (R_p) derived from the potentiodynamic polarization plots depicted in Fig. 5 are given in Table 5.
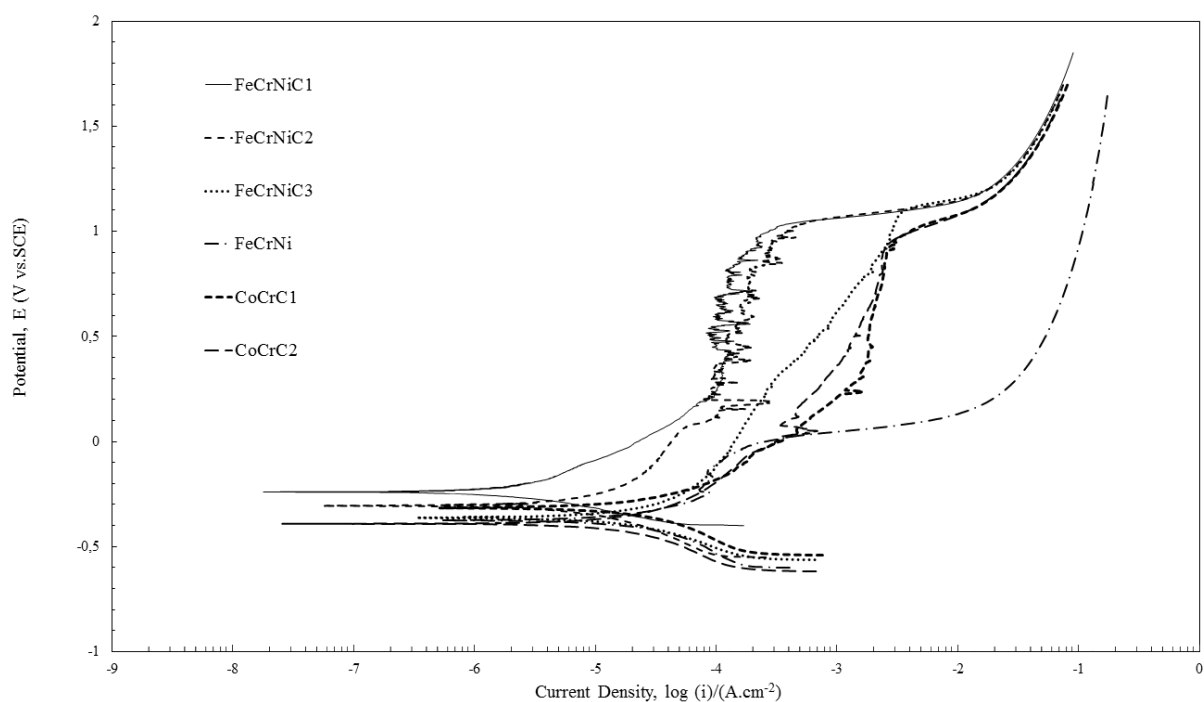

Fig. 5. Potentiodynamic polarization plots of various Fe- and Co-based coatings immersed in 3.5% NaCl, at 25°C.

Table 5. Electrochemical values of the coated and uncoated steel substrate, immersed in 3.5% NaCl, at 25°C

Coding	i_{corr} (μAcm^{-2})	E_{corr} (V vs. SCE)	b_a (V dec^{-1})	b_c (V dec^{-1})	R_p (kΩcm^2)
FeCrNiC1	0.9	-0.25	0.26	0.18	43.9
FeCrNiC2	1.9	-0.31	0.21	0.13	18.3
FeCrNiC3	9.4	-0.36	0.24	0.16	4.4
FeCrNi	7.7	-0.37	0.16	0.09	3.2
CoCrC1	8.1	-0.32	0.17	0.14	4.1
CoCrC2	4.7	-0.38	0.12	0.11	5.3

Apart from the FeCrNiC1 coating with noble potential of -0.25V, the E_{corr} of the other coatings varied from -0.31 to -0.38V, showing negligible differences between those samples thermodynamically. The i_{corr} varied from 0.9 to 9.4 µAcm^{-2}. FeCrNi coating showed high passive current density (i_{pass}) combined with a narrow passive region and it even underwent active dissolution at the low potential without any visible passivation.

The lowest corrosion current density was observed for FeCrNiC1 (0.9 µAcm^{-2}), which is due to the formation of a stable and protective superficial layer. Furthermore, it was not possible to find a direct correlation between coating defect and i_{corr}, probably because the elemental composition in addition to the defects can play a significant role in corrosion processes.

It can be seen in Fig. 5 that FeCrNiC3 and CoCrC1 coatings illustrated passivation stage at a relatively high i_{pass}, which could be attributed to the structural defects of coatings including pores and microcracks occasionally appeared. FeCrNi coating showed similar behavior which might be associated with the lamellar characteristics of the coating. The presence of the lamella boundaries hinders the outward migration of Cr to reach the top surface of the coating which eventually leads to weak passivation. FeCrNiC1 and FeCrNiC2 coatings exhibited passivation stage at low i_{corr} with some tiny fluctuations. The fluctuation of the passive region implied continuous process of active solution and passivation. The transpassive potential (E_{trans}) of these coatings was about 1.0V combined with a broad passive region, which confirmed that these coatings had an ability to prevent localized corrosion. Contrarily, the very limited passive region of FeCrNi coating illustrated a low ability to hinder localized corrosion. In Co-based coatings, E_{corr} was lower than that of FeCrNiC coatings, which confirmed these coatings were more active in galvanic couples. The passivation stage of Co-based coatings occurred at higher i_{corr} compared to FeCrNiC coatings, implying a poor ability for the surface passive films to be stable. However, broad passive regions were identified by similarly high E_{trans}, 1.0V, as observed in FeCrNiC coatings. Therefore, Fe-based coatings, especially FeCrNiC1, could be efficient as

a protective barrier and keep the excellent corrosion properties to prevent localized corrosion in such environments.

High resistance to localized corrosion such as pitting of the high-alloyed Fe-based coatings was considered to be determined by the presence of Cr-rich passive surface films formed on the Fe-based coatings, which prevented further attack by the corrosive solution. Moreover, Mo content of the coating could also reduce the possibility of pitting, improve the corrosion resistance and passivating ability, since it prevented the dissolution of Cr during passivation [46]. FeCrNiC1 and FeCrNiC2, which contained high amounts of Cr, Mo and Ni, were observed to have very low i_{corr} and, thereby, high resistance to corrosion. Hence, it is indicated that the corrosion resistance of the Fe-based coatings was sensitive to the microstructure characteristic identified by spraying parameters.

It could be hypothesized that "passive-like" stages were produced due to the formation of a thin passive oxide film; however, defects e.g., pores, oxide inclusions and interlamellar boundaries led to a disruption in perfect passivity. The initial breakaway of "passive-like" stage might be connected to the galvanic microcells or selective corrosion along lamellae boundaries, based on the mechanism identical to pitting. The former produces quite low damage; therefore, it can be attributed to lower anodic i_{corr}; instead, the latter inflicts more damage, resulting in higher anodic i_{corr}.

Regarding the polarization resistance calculated in Table 5, the largest R_p was consistently reported for FeCrNiC1 (43.9 kΩcm^2) due to the low i_{corr} and quite high β_a and β_c. Indeed, high β_a and β_c lead to lower anodic and cathodic current at the same overpotential during the polarization measurements which consequently results in higher R_p.

3.4. EIS

EIS is a non-destructive method which relies on small AC-voltage signal (20 mV) and applicable to study the resistance and capacitance of the coatings through a fit of the data based on a

proper model circuit. Fig. 6 (a and b) showed Nyquist and Bode diagrams of coatings in 3.5 wt.% NaCl solution. During the exposure, corrosive ions penetrated the defects through the coating before reaching the substrate. Thus, at the beginning of the test, the electrochemical behavior could be associated with the intrinsic properties of the coating.
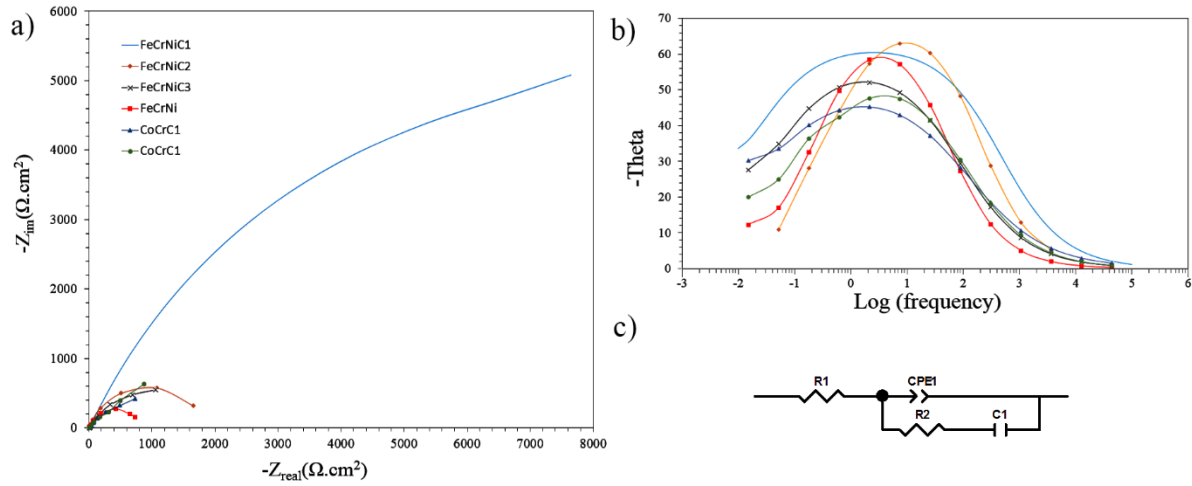

Fig. 6. a) Nyquist and b) Bode diagrams for HVAF coated samples in 3.5% NaCl, at 25°C, c) Equivalent electric circuit for all coatings.

EIS results illustrated the presence of one capacitive loop for all coatings. The diameter of this capacitance loop can be linked to the corrosion resistance. The fact that only one single time constant was gained might be less likely due to the short exposure time. Moreover, it could also be considered that the electrolyte failed to penetrate through the whole thickness of the coating and meet the coating/substrate interface. Thus, the electrochemical characteristics derived from EIS measurements could be attributed to the Faradaic process (as a result of charge transfer across an interface) that comprised the coating reactivity [47].

Whereas the defects such as pores were fine, the formation of corrosion products due to some corrosion reactions within the coating or at the interface, allowed to pore partial sealing [48]. However, these corrosion products had poor adherence, which eventually leads the electrolyte to penetrate further through the pores.

Consequently, a simple equivalent circuit to describe the electrochemical behavior of coatings was suggested, as shown in Fig. 6 c. The equivalent circuits included the solution resistance (R_s), charge transfer resistance in the coating/solution interface (R_{ct}), coating double-layer capacitance (C_{dl}) described by a constant phase element (*CPE*).

The corrosion parameters derived from the equivalent electric circuit are given in Table 6. R_{ct} describes the ability of the coating to inhibit ion transfer at the solution/coating interface. It can be observed that R_{ct} decreased with the increase of defects within the coating and most likely due to the dissolution of oxides because of chloride ion adsorption and chloride attack to the passive film. The higher R_{ct} confirmed the lower exposed coating/electrolyte interface and therefore lower coating open porosity and accordingly lower corrosion of the coating. Therefore, better corrosion resistance of the FeCrNiC1 coating compared to both Co-based coatings was confirmed. Furthermore, better corrosion protection properties of the high-alloyed Fe-based coating (FeCrNiC1) compared to the low-alloyed Fe-based (FeCrNi) in 3.5 wt.% NaCl solution were verified. The figure confirms that the presence of more Cr in FeCrNiC effectively decreased the corrosion.

Table 6. Electrochemical parameters gained from EIS spectra of HVAF coated samples

Coating	R_s (Ωcm^2)	R_{ct} ($k\Omega cm^2$)	CPE-T (μFcm^{-2})	n	C_{dl} (μFcm^{-2})
FeCrNiC1	9.9	20.1	0.05	0.79	120
FeCrNiC2	10.2	6.8	0.17	0.80	4000
FeCrNiC3	9.9	4.4	0.07	0.78	5020
FeCrNi	10.0	0.8	0.05	0.79	925
CoCrC1	10.0	2.1	0.08	0.76	5115
CoCrC2	10.1	2.8	0.08	0.75	5040

CPE is generally employed to model the behavior of double layer in real electrochemical processes [49]. *CPE* means the double layer capacitance at the solution/coating interface which includes the interfaces between the top surface of the coating and the solution and also the surface of defects with the solution. Furthermore, the value of *CPE* suggested that the porosity increased during the immersion, accordingly, due to the penetration of the solution. The "plugging effect" resulted from the accumulation of corrosion products in defects might be a reason for the increase in *CPE* [2, 28].

The time constants *n* of all the coatings attributed to the charge transfer reaction were relatively similar, confirming that the same electrochemical mechanism happened. By definition the capacitance has direct relation with the electrical permittivity of the material and to the total plate area and inverse relation with the distance between the two conductive plates. Since the electrical permittivity of the 3.5wt.% NaCl solution and the distance (the thickness of the electrical double layer formed on the coating surface) and were fixed, a decrease of the double layer capacitance might be associated with the lower electrolyte penetration (i.e., lower overall area) and thus, lower open porosity [24].

3.5. Surface morphology

Figs. 7 and 8 showed the morphology of the surface coatings after 24-hour immersion in OCP test for the coating of each group that experienced the highest corrosion (FeNiCrC3 and CoCrC1) to clarify the corrosion mechanism of the coating.
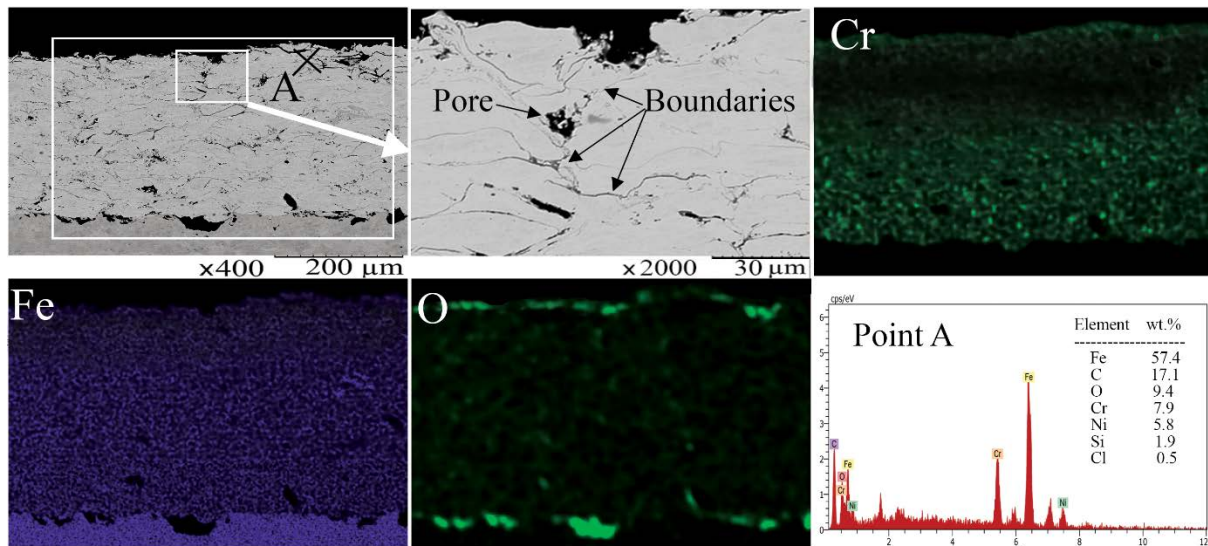
Fig. 7. Microstructure, elemental mapping and point EDS analysis of the corroded FeNiCrC3 coating after 24-hour OCP test, at 25°C.
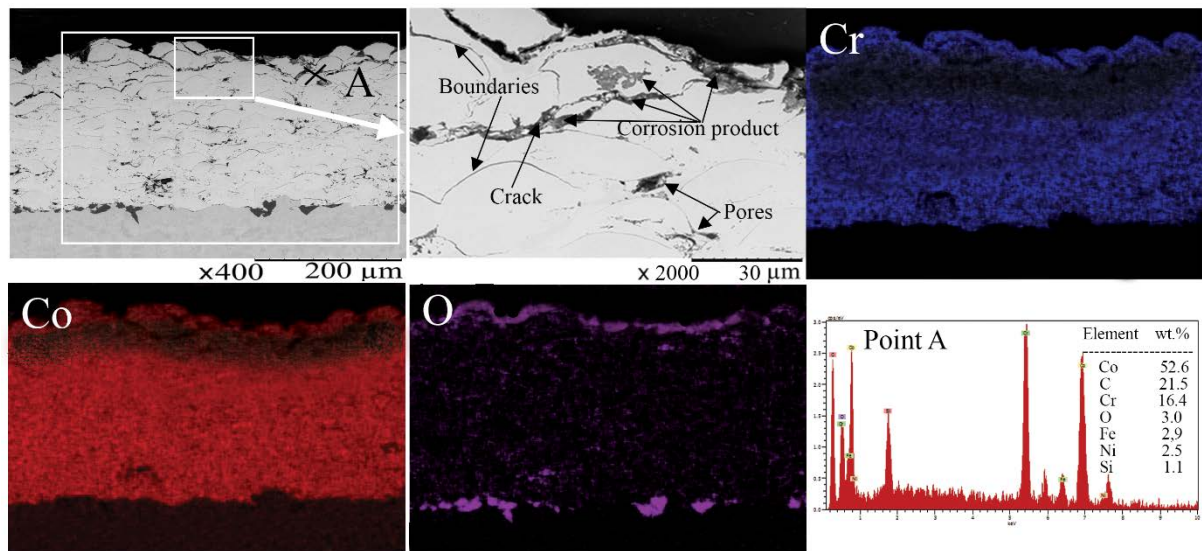

Fig. 8. Microstructure, elemental mapping and point EDS analysis of the corroded CoCrC1 coating after 24-hour OCP test, at 25°C.

The corrosion mechanism was similar to crevice or pitting corrosion and the pores in the coating acted as blocked cells, which had catalytic influences on the corrosion reactions, as the diffusion of O_2 molecules into these defects was much slower than that of small Cl^-. Additionally, the oxygen depletion causes a fast decline of the electrolyte pH in the crevice [7]. The Cl^- penetrated into the crevices favors hydrolysis reactions, which further decreased the electrolyte pH. Over

time, the inner corrosion products of Fe^{2+} or Co^{2+} migrated to the coating surface, where the hydroxide was generated.

It can be observed that in both coatings, the most severe corrosion damage occurred along the lamellar boundaries on the top surface of the coating, where several factors affect the corrosion behavior; initially, as defects e.g., pores or weak interlamellar cohesion were present in coating surface, they became preferential sites for corrosion nucleation. Moreover, cracks along lamellae boundaries became preferential sites for corrosion growth. In both coatings, the defects e.g., pores, microcracks, and lamellar structures served as open channels, which eventually led to a direct path between the electrolyte and inside part of the coating. In FeCrNiC3 (Fig. 7), the formation of passive film due to the presence of Cr in the coating prevented the easy penetration of corrosive species to reach the substrate. Thus, it presented better corrosion resistance in contrast to the CoCrC1 coating.

4. Conclusions

The corrosion behavior of HVAF thermally sprayed Fe- and Co-based coatings was studied using electrochemical measurements. The major conclusions taken from the work can be summarized as follows:

1) Powders with coarse particle size (20-53 μm) were successfully sprayed by HVAF process.

2) The high-alloyed Fe-based coating effectively protected the underlying substrate better than both low-alloyed Fe-based and Co-based coatings. The corrosion resistance of the Fe-based coatings significantly increased by adding Cr.

3) Altering the coating thickness was a way that can change the diffusion of the corrosive electrolyte. Thin Co-based coating permitted the corrosive ions to diffuse, while thin Fe-based coating showed better results compared with thick Fe-based coating.

4) Increasing the in-flight Fe-based particle temperature from 1400°C to 1515°C provided a denser coating, which eventually improved the corrosion resistance of the sample.

5) The preferred sites for corrosion nucleation and growth were defects e.g., pores, cracks and interlamellar boundaries.

6) The high-alloyed Fe-based coatings which showed a better corrosion behavior are recommended as a potential alternative to Co-based coatings.

5. Conflict of interest

The authors declare that there is no conflict of interest regarding the publication of this paper.

6. References

[1]   X. Q. Liu, Y. G. Zheng, X. C. Chang, W. L. Hou, J. Q. Wang, Z. Tang, and A. Burgess, "Microstructure and properties of Fe-based amorphous metallic coating produced by high velocity axial plasma spraying," *J. Alloys Compd.*, vol. 484, no. 1–2, pp. 300–307, Sep. 2009.

[2]   R. Q. Guo, C. Zhang, Y. Yang, Y. Peng, and L. Liu, "Corrosion and wear resistance of a Fe-based amorphous coating in underground environment," *Intermetallics*, vol. 30, pp. 94–99, Nov. 2012.

[3]   W. Lu, Y. Wu, J. Zhang, S. Hong, J. Zhang, and G. Li, "Microstructure and Corrosion Resistance of Plasma Sprayed Fe-Based Alloy Coating as an Alternative to Hard Chromium," *J. Therm. Spray Technol.*, vol. 20, no. 5, pp. 1063–1070, Dec. 2010.

[4]   C. S. Brandolt, M. R. Ortega Vega, T. L. Menezes, R. M. Schroeder, and C. F. Malfatti, "Corrosion behavior of nickel and cobalt coatings obtained by high-velocity oxy-fuel (HVOF) thermal spraying on API 5CT P110 steel," *Mater. Corros.*, p. n/a–n/a, Sep. 2015.

[5]   W.-H. Liu, F.-S. Shieu, and W.-T. Hsiao, "Enhancement of wear and corrosion resistance of iron-based hard coatings deposited by high-velocity oxygen fuel (HVOF) thermal spraying," *Surf. Coat. Technol.*, vol. 249, pp. 24–41, Jun. 2014.

[6]   Y. Gao, J. Xiong, D. Gong, J. Li, and M. Ding, "Improvement of solar absorbing property of Ni–Mo based thermal spray coatings by laser surface treatment," *Vacuum*, vol. 121, pp. 64–69, Nov. 2015.

[7]   J. A. Picas, E. Rupérez, M. Punset, and A. Forn, "Influence of HVOF spraying parameters on the corrosion resistance of WC–CoCr coatings in strong acidic environment," *Surf. Coat. Technol.*, vol. 225, pp. 47–57, Jun. 2013.

[8]   V. R. S. Sá Brito, I. N. Bastos, and H. R. M. Costa, "Corrosion resistance and characterization of metallic coatings deposited by thermal spray on carbon steel," *Mater. Des.*, vol. 41, pp. 282–288, Oct. 2012.

[9]   L.-M. Berger, "Application of hardmetals as thermal spray coatings," *Int. J. Refract. Met. Hard Mater.*, vol. 49, pp. 350–364, Mar. 2015.

[10]   A. Milanti, H. Koivuluoto, and P. Vuoristo, "Influence of the Spray Gun Type on Microstructure and Properties of HVAF Sprayed Fe-Based Corrosion Resistant Coatings," *J. Therm. Spray Technol.*, vol. 24, no. 7, pp. 1312–1322, Sep. 2015.

[11]   Z. ZHOU, L. WANG, F. WANG, and Y. LIU, "Formation and corrosion behavior of Fe-based amorphous metallic coatings prepared by detonation gun spraying," *Trans. Nonferrous Met. Soc. China*, vol. 19, Supplement 3, pp. s634–s638, Dec. 2009.

[12]   G. Bolelli, B. Bonferroni, J. Laurila, L. Lusvarghi, A. Milanti, K. Niemi, and P. Vuoristo, "Micromechanical properties and sliding wear behaviour of HVOF-sprayed Fe-based alloy coatings," *Wear*, vol. 276–277, pp. 29–47, Feb. 2012.

[13]   C. Zhang, L. Liu, K. C. Chan, Q. Chen, and C. Y. Tang, "Wear behavior of HVOF-sprayed Fe-based amorphous coatings," *Intermetallics*, vol. 29, pp. 80–85, Oct. 2012.

[14]   J. Farmer, J.-S. Choi, C. Saw, J. Haslam, D. Day, P. Hailey, T. Lian, R. Rebak, J. Perepezko, J. Payer, D. Branagan, B. Beardsley, A. D'amato, and L. Aprigliano, "Iron-Based Amorphous Metals: High-Performance Corrosion-Resistant Material Development," *Metall. Mater. Trans. A*, vol. 40, no. 6, pp. 1289–1305, Mar. 2009.

[15]   D. R. Maddala and R. J. Hebert, "Sliding wear behavior of Fe50−xCr15Mo14C15B6Erx (x=0, 1, 2 at%) bulk metallic glass," *Wear*, vol. 294–295, pp. 246–256, Jul. 2012.

[16]   W. Guo, Y. Wu, J. Zhang, S. Hong, G. Li, G. Ying, J. Guo, and Y. Qin, "Fabrication and Characterization of Thermal-Sprayed Fe-Based Amorphous/Nanocrystalline Composite Coatings: An Overview," *J. Therm. Spray Technol.*, vol. 23, no. 7, pp. 1157–1180, Apr. 2014.

[17] M. M. Qiu, H. Wang, X. Wu, H. Q. Tang, and G. C. Su, "Study on the Corrosion Resistance of High Boron Iron-Based Alloy," *Appl. Mech. Mater.*, vol. 268–270, pp. 326–329, Dec. 2012.

[18] V. Pokhmurskii, M. Student, V. Gvozdeckii, T. Stypnutskyy, O. Student, B. Wielage, and H. Pokhmurska, "Arc-Sprayed Iron-Based Coatings for Erosion-Corrosion Protection of Boiler Tubes at Elevated Temperatures," *J. Therm. Spray Technol.*, vol. 22, no. 5, pp. 808–819, Apr. 2013.

[19] S. D. Zhang, W. L. Zhang, S. G. Wang, X. J. Gu, and J. Q. Wang, "Characterisation of three-dimensional porosity in an Fe-based amorphous coating and its correlation with corrosion behaviour," *Corros. Sci.*, vol. 93, pp. 211–221, Apr. 2015.

[20] S. Katakam, J. Y. Hwang, S. Paital, R. Banerjee, H. Vora, and N. B. Dahotre, "In Situ Laser Synthesis of Fe-Based Amorphous Matrix Composite Coating on Structural Steel," *Metall. Mater. Trans. A*, vol. 43, no. 13, pp. 4957–4966, Jul. 2012.

[21] T. Lampke, B. Wielage, H. Pokhmurska, C. Rupprecht, S. Schuberth, R. Drehmann, and F. Schreiber, "Development of particle-reinforced nanostructured iron-based composite alloys for thermal spraying," *Surf. Coat. Technol.*, vol. 205, no. 12, pp. 3671–3676, Mar. 2011.

[22] R. Li, Z. Li, Y. Zhu, and K. Qi, "Structure and corrosion resistance properties of Ni–Fe–B–Si–Nb amorphous composite coatings fabricated by laser processing," *J. Alloys Compd.*, vol. 580, pp. 327–331, Dec. 2013.

[23] G. Bolelli, L.-M. Berger, T. Börner, H. Koivuluoto, L. Lusvarghi, C. Lyphout, N. Markocsan, V. Matikainen, P. Nylén, P. Sassatelli, R. Trache, and P. Vuoristo, "Tribology of HVOF- and HVAF-sprayed WC–10Co4Cr hardmetal coatings: A comparative assessment," *Surf. Coat. Technol.*, vol. 265, pp. 125–144, Mar. 2015.

[24] A. Milanti, V. Matikainen, H. Koivuluoto, G. Bolelli, L. Lusvarghi, and P. Vuoristo, "Effect of spraying parameters on the microstructural and corrosion properties of HVAF-sprayed Fe–Cr–Ni–B–C coatings," *Surf. Coat. Technol.*, vol. 277, pp. 81–90, Sep. 2015.

[25] Z. B. Zheng, Y. G. Zheng, W. H. Sun, and J. Q. Wang, "Erosion–corrosion of HVOF-sprayed Fe-based amorphous metallic coating under impingement by a sand-containing NaCl solution," *Corros. Sci.*, vol. 76, pp. 337–347, Nov. 2013.

[26] I. Hulka, V. A. Şerban, I. Secoşan, P. Vuoristo, and K. Niemi, "Wear properties of CrC–37WC–18M coatings deposited by HVOF and HVAF spraying processes," *Surf. Coat. Technol.*, vol. 210, pp. 15–20, Oct. 2012.

[27] Q. Wang, S. Zhang, Y. Cheng, J. Xiang, X. Zhao, and G. Yang, "Wear and corrosion performance of WC-10Co4Cr coatings deposited by different HVOF and HVAF spraying processes," *Surf. Coat. Technol.*, vol. 218, pp. 127–136, Mar. 2013.

[28] R. Q. Guo, C. Zhang, Q. Chen, Y. Yang, N. Li, and L. Liu, "Study of structure and corrosion resistance of Fe-based amorphous coatings prepared by HVAF and HVOF," *Corros. Sci.*, vol. 53, no. 7, pp. 2351–2356, Jul. 2011.

[29] C.-J. Li and G.-J. Yang, "Relationships between feedstock structure, particle parameter, coating deposition, microstructure and properties for thermally sprayed conventional and nanostructured WC–Co," *Int. J. Refract. Met. Hard Mater.*, vol. 39, pp. 2–17, Jul. 2013.

[30] S. Liu, D. Sun, Z. Fan, H. Yu, and H. Meng, "The influence of HVAF powder feedstock characteristics on the sliding wear behaviour of WC–NiCr coatings," *Surf. Coat. Technol.*, vol. 202, no. 20, pp. 4893–4900, Jul. 2008.

[31] A. P. Wang, Z. M. Wang, J. Zhang, and J. Q. Wang, "Deposition of HVAF-sprayed Ni-based amorphous metallic coatings," *J. Alloys Compd.*, vol. 440, no. 1–2, pp. 225–228, Aug. 2007.

[32] W. Yingjie, O. Gengsheng, Z. Lei, W. Xiaoping, Z. Hengyu, and W. Shanlin, "Corrosion Resistance of Coating with Fe-based Metallic Glass Powders Fabricated by Laser Spraying," *J. Appl. Sci.*, vol. 13, no. 9, pp. 1479–1483, Sep. 2013.

[33] R. Manish, *Thermal Sprayed Coatings and their Tribological Performances*. IGI Global, 2015.

[34] Y. Wang, Z. Z. Xing, Q. Luo, A. Rahman, J. Jiao, S. J. Qu, Y. G. Zheng, and J. Shen, "Corrosion and erosion–corrosion behaviour of activated combustion high-velocity air fuel sprayed Fe-based amorphous coatings in chloride-containing solutions," *Corros. Sci.*, vol. 98, pp. 339–353, Sep. 2015.

[35] G. Bolelli, T. Börner, A. Milanti, L. Lusvarghi, J. Laurila, H. Koivuluoto, K. Niemi, and P. Vuoristo, "Tribological behavior of HVOF- and HVAF-sprayed composite coatings based on Fe-Alloy + WC–12% Co," *Surf. Coat. Technol.*, vol. 248, pp. 104–112, Jun. 2014.

[36] C. Lyphout and K. Sato, "Screening design of hard metal feedstock powders for supersonic air fuel processing," *Surf. Coat. Technol.*, vol. 258, pp. 447–457, Nov. 2014.

[37] C. A. Schneider, W. S. Rasband, and K. W. Eliceiri, "NIH Image to ImageJ: 25 years of image analysis," *Nat. Methods*, vol. 9, no. 7, pp. 671–675, Jul. 2012.

[38] D. A. Jones, *Principles and Prevention of Corrosion: Pearson New International Edition*. Pearson Education, Limited, 2013.

[39] A. Milanti, H. Koivuluoto, P. Vuoristo, G. Bolelli, F. Bozza, and L. Lusvarghi, "Microstructural Characteristics and Tribological Behavior of HVOF-Sprayed Novel Fe-Based Alloy Coatings," *Coatings*, vol. 4, no. 1, pp. 98–120, Jan. 2014.

[40] W.-M. Zhao, Y. Wang, L.-X. Dong, K.-Y. Wu, and J. Xue, "Corrosion mechanism of NiCrBSi coatings deposited by HVOF," *Surf. Coat. Technol.*, vol. 190, no. 2–3, pp. 293–298, Jan. 2005.

[41] H. J. C. Voorwald, L. F. S. Vieira, and M. O. H. Cioffi, "Evaluation of WC-10Ni thermal spraying coating by HVOF on the fatigue and corrosion AISI 4340 steel," *Procedia Eng.*, vol. 2, no. 1, pp. 331–340, Apr. 2010.

[42] S. M. Lee, W. G. Lee, Y. H. Kim, and H. Jang, "Surface roughness and the corrosion resistance of 21Cr ferritic stainless steel," *Corros. Sci.*, vol. 63, pp. 404–409, Oct. 2012.

[43] V. A. D. Souza and A. Neville, "Linking electrochemical corrosion behaviour and corrosion mechanisms of thermal spray cermet coatings (WC–CrNi and WC/CrC–CoCr)," *Mater. Sci. Eng. A*, vol. 352, no. 1–2, pp. 202–211, Jul. 2003.

[44] C. Zhang, K. C. Chan, Y. Wu, and L. Liu, "Pitting initiation in Fe-based amorphous coatings," *Acta Mater.*, vol. 60, no. 10, pp. 4152–4159, Jun. 2012.

[45] L. Liu and C. Zhang, "Fe-based amorphous coatings: Structures and properties," *Thin Solid Films*, vol. 561, pp. 70–86, Jun. 2014.

[46] L. Zhao and E. Lugscheider, "Influence of the spraying processes on the properties of 316L stainless steel coatings," *Surf. Coat. Technol.*, vol. 162, no. 1, pp. 6–10, Jan. 2003.

[47] S. Brioua, K. Belmokre, V. Debout, P. Jacquot, E. Conforto, S. Touzain, and J. Creus, "Corrosion behavior in artificial seawater of thermal-sprayed WC-CoCr coatings on mild steel by electrochemical impedance spectroscopy," *J. Solid State Electrochem.*, vol. 16, no. 2, pp. 633–648, May 2011.

[48] Y. Yang, C. Zhang, Y. Peng, Y. Yu, and L. Liu, "Effects of crystallization on the corrosion re-sistance of Fe-based amorphous coatings," *Corros. Sci.*, vol. 59, pp. 10–19, Jun. 2012.

[49] J. Zhang and V. Desai, "Evaluation of thickness, porosity and pore shape of plasma sprayed TBC by electrochemical impedance spectroscopy," *Surf. Coat. Technol.*, vol. 190, no. 1, pp. 98–109, Jan. 2005.

[50] G. Bolelli, I. Hulka, H. Koivuluoto, L. Lusvarghi, A. Milanti, K. Niemi, and P. Vuoristo, "Properties of WC–FeCrAl coatings manufactured by different high velocity thermal spray processes," *Surf. Coat. Technol.*, vol. 247, pp. 74–89, May 2014.